# Desulfurization Performance of MgO/ Rice Straw Biochar Adsorbent Prepared by Co-precipitation/ Calcination Route

Jiali Chen, Lianhan Huang, Liming Sun, and Xiaofan Zhu *

A solid adsorbent for $SO_2$ adsorption was prepared from magnesium salt/rice straw *via* co-precipitation/calcination. The effects of various preparation conditions, including the calcination temperature, the weight ratio of Mg/rice straw, magnesium salts, and amine precipitants, were investigated relative to their effects on the desulfurization performance of adsorbents. Maximum sulfur adsorption capacity (260 mg/g) was obtained with MgO/rice straw biochar adsorbent using tetraethylenepentamine (TEPA) as the precipitants, and the preparation conditions included a calcination temperature of 400 °C, a Mg/rice straw weight ratio of 1.2, and magnesium chloride hexahydrate ($MgCl_2 \cdot 6H_2O$) as the magnesium source. The rice straw biochar-supported MgO sample displayed a high $SO_2$ adsorption capacity due to its excellent textural properties, large specific surface areas, small crystallite size, numerous surface active sites of MgO nanoparticles, and introduced N-H groups. The physical and chemical properties of samples were investigated by field emission scanning electron microscopy (FESEM), Brunauer-Emmett-Teller (BET) analyses, Fourier transform infrared spectrometer (FT-IR), elemental analysis (EA), and X-ray diffraction (XRD).

*Keywords: Rice straw; Biochar; MgO; Co-precipitation/calcination; Sulfur dioxide; Adsorption*

*Contact information: Analytical and Testing Center, Sichuan University, Chengdu 610065, China;*
** Corresponding author: zxf62@scu.edu.cn*

## INTRODUCTION

Sulfur dioxide ($SO_2$) is the main component of acid rain, and its corrosive properties have detrimental effects on both the environment and human health, making it urgent to reduce $SO_2$ emissions. Among the various flue gas desulfurization technologies to remove $SO_2$, the adsorption methods have shown promising characteristics because of its advantages of simple operation procedures, low energy consumption for regeneration, little or no water consumption, lack of secondary pollution, no volatility or corrosion issues, and a wide variety of adsorbents (Mochida *et al*. 2000; Tailor *et al*. 2014a). Popular solid adsorbents include activated carbon (Yan *et al*. 2012, 2013; Guo *et al*. 2013; Yi *et al*. 2014), carbon fibers (Zhou *et al*. 2012; Bai *et al*. 2016), zeolites (Al-Harahsheh *et al*. 2014; Vellingiri *et al*. 2016), polymer-supported metal oxides (Wang *et al*. 2009), and metal-supported materials (Guo *et al*. 2012; Li *et al*. 2012), and metal–organic frameworks (MOFs) (Savage *et al*. 2016; Tan *et al*. 2017; Elder *et al*. 2018; Wang *et al*. 2018). Magnesium oxide (MgO) nano-materials have attracted significant attention due to their large surface areas, plentiful surface active sites, and excellent adsorption properties (Dhal *et al*. 2015; Li *et al*. 2017). MgO combined with activated carbon has been used also to adsorb dyes (Liu *et al*. 2015; Nassar *et al*. 2017), $CO_2$ (Vu *et al*. 2016), fluoride (Jin *et al*. 2016), phosphates (Zhou *et al*. 2011), and toxic heavy metal ions (Chowdhury *et al*. 2016). Furthermore, the alkalinity of MgO, an alkaline earth metal oxide, has strong adsorption

ability for acidic $SO_2$ gas.

Currently, large amounts of rice straw residues are discarded or burned in the open air without effective utilization, which causes serious environmental pollution. As a result, effective and environmentally-friendly methods for taking advantage of rice straw should be developed. Modifying rice straw *via* catalytic oxidation, followed by alkaline nitrogen reagents treatment results in effective $SO_2$ adsorption (Yang *et al*. 2012; Sun and Zhu 2018). However, the modification methods have some drawbacks; they are not suitable for high temperature, require a complicated process, and have a poor regeneration effect. Hence, biochar derived from waste biomass is widely used as an adsorbent due to its stability and high sorption ability. Biochar has similar pore structure and surface chemical property as activated carbon, and its simple preparation process and low investment used as a potential adsorption substitute for activated carbon (Ahmad *et al*. 2014). Biochar derived from waste biomass has a highly porous structure and contain various functional groups that are effective in the adsorption of metals (Wu *et al*. 2012) and $CO_2$ capture (Huang *et al*. 2015). Meanwhile, biochar is a carbon-rich adsorbent with inorganic constituents, which has enormous potential sorption ability for $SO_2$ (Xu *et al*. 2016).

This paper exhibits a new synthetic route to obtain rice straw biochar-loaded magnesium oxide (RSB-MgO) materials by co-precipitating and calcining magnesium salt /rice straw using amine reagents as precipitants. The effects of preparation conditions were investigated, including calcination temperature, the weight ratios of Mg/rice straw, magnesium salts, and amine-containing precipitants. The adsorption temperature and simulated flue gas flow rate were also studied. The prepared RSB-MgO adsorbents were characterized using field emission scanning electron microscopy (FESEM), Brunauer-Emmett-Teller (BET) analyses, Fourier transform infrared spectrometer (FT-IR), element analysis (EA), and X-ray diffraction (XRD).

## EXPERIMENTAL

### Materials and Reagents

Rice straw specimens were collected from farmland in Chengdu, Sichuan Province, China. Magnesium chloride hexahydrate ($MgCl_2 \cdot 6H_2O$), magnesium nitrate hexahydrate ($Mg(NO_3)_2 \cdot 6H_2O$), magnesium acetate tetrahydrate ($Mg(CH_3COO)_2 \cdot 4H_2O$), ethylene-diamine (EDA), tetraethylenepentamine (TEPA), diethanolamine (DEA), 30% hydrogen peroxide ($H_2O_2$), sodium hydroxide (NaOH), bromocresol green, and methyl red indicators were used as raw materials. All reagents were analytical grade and used without further purification. They were supplied from Ke Long Chemical Reagent Company (Chengdu, China), except for magnesium acetate tetrahydrate (Mg $(CH_3COO)_2 \cdot 4H_2O$), which was obtained from Aladdin Industrial Corporation. The carrier gas (compressed air, Sichuan Peace Gas Co., Ltd., China), simulated flue gas ($SO_2/N_2$~0.3%, Chengdu Jin Ke Xing Gas Co., Ltd., China), vacuum tube high-temperature sintering furnace (OTF-1200X, Ke Jing Material Technology Co., Ltd., China).

### Preparation of RSB-MgO Adsorbent

Rice straw was crushed into powder and passed through a 20-mesh sieve. $MgCl_2 \cdot 6H_2O$ (200 mL, 0.01 M) ($MgCl_2 \cdot 6H_2O$ = 20.33 g) and 2.0 g rice straw powder were mixed in a beaker (250 mL) in a 60 °C water bath. EDA was added dropwise to the solution with continuous stirring until the pH reached 11. The reaction was stirred for 1 h and then

allowed to stand for 3 h at room temperature. The precipitate was dried at 105 °C for 2 h, then calcined in a high-temperature vacuum sintering furnace to obtain RSB-MgO adsorbent. The calcination conditions were as follows: compressed air gas (180 mL/min) was used as the carrier gas, a heating rate of 15 °C /min, and a calcination time of 1 h at 400 °C. The schematic diagram for the preparation of RSB-MgO is shown in Fig. 1.

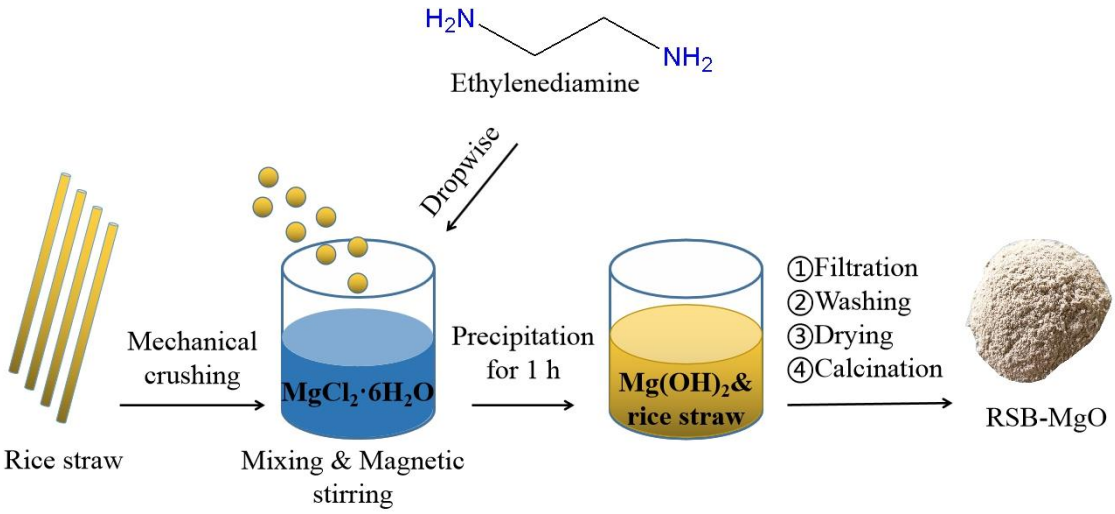


**Fig. 1.** Schematic of the preparation of RSB-MgO adsorbent through precipitation with amine agents and high temperature calcination

## Characterization

The morphology of RSB-MgO adsorbent was characterized by FESEM (JSM-7500F, JEOL, Tokyo, Japan). The phase retrieval and grain sizes were obtained by XRD (EMPYREAN, PANalytical B.V, Almelo, Netherlands). Specific surface areas, pore volumes, and average pore diameters were measured using a Brunauer–Emmett–Teller (BET) surface area analyzer (Fully automatic specific surface and micro-pore size analyzer, 3Flex, Micromeritics, Norcross, GA, USA). FT-IR analyses were conducted using an FT-IR spectrometer (Nicolet 6700, Thermo Electron Corporation, Waltham, MA, USA). The elemental compositions of samples were investigated by element analyzer (EURO EA3000, Elementar Analysen-systeme GmbH, Langenselbold, Germany).

## Adsorption Experiments

First, 1.0 g of RSB-MgO was loaded onto a glass adsorption column (Φ30 mm × 300 mm) in a 25 °C water bath. The simulated flue gas with an inlet $SO_2$ concentration (initial $SO_2$ concentration, 0.3% volume concentration) was passed through the adsorption column at a flow rate of 400 mL·min$^{-1}$. The adsorption experiment was considered complete when the $SO_2$ concentration in the exhaust gas exceeded 80% of the inlet $SO_2$ concentration (*i.e.*, when the desulfurization efficiency decreased to 20%). The $SO_2$ in the exhaust gas was absorbed by $H_2O_2$ (3%) solution and titrated by NaOH (0.01 M) to neutrality. Sulfur adsorption capacity is used to indicate the $SO_2$ adsorption capacity of a sample, and the desulfurization efficiency (Eq. 1) and sulfur adsorption capacity (Eq. 2) were calculated according to the following formulas,

$$\eta = \frac{C_{\text{in}} - C_{\text{out}}}{C_{\text{in}}} \times 100\% \quad (1)$$

$$Cs = \frac{\int_0^{t_{20\%}} Q \times \eta \times C_{\text{in}} \text{d}t}{\text{m}} \quad (2)$$

where $\eta$ is the desulfurization efficiency (%); $C_{in}$ is the inlet $SO_2$ concentration of the simulated flue gas (ppm); $C_{out}$ is the outlet concentration of $SO_2$ in the exhaust gas (ppm); $C_s$ is the sulfur adsorption capacity ($mg \cdot g^{-1}$); $m$ is the weight of adsorbent (g); $Q$ is the gas flow rate ($L \cdot min^{-1}$); and $t_{20\%}$ is the contact time when the desulfurization efficiency decreased to 20% (min). The flow chart of $SO_2$ adsorption is shown in Fig. 2.

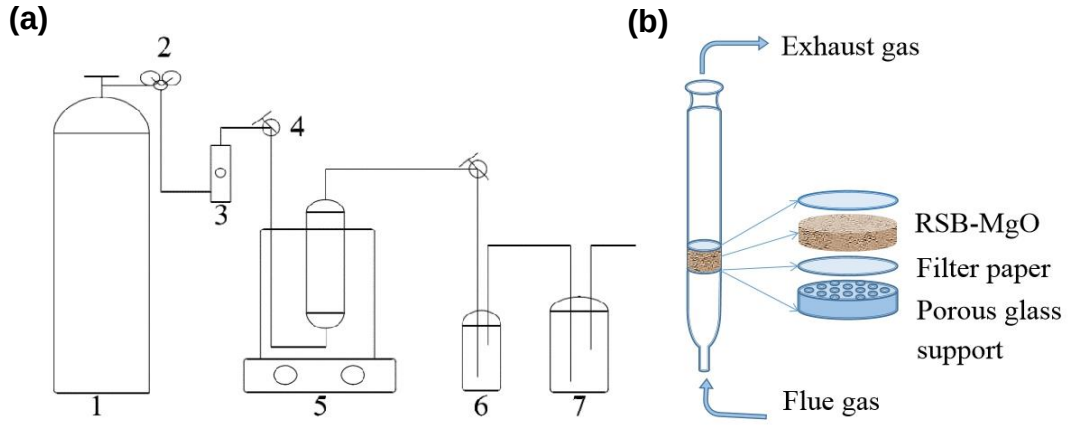


**Fig. 2.** (a) $SO_2$ adsorption apparatus. Gas supply system: 1. $SO_2/N_2$ 0.3%, 2. Pressure reducing valve, 3. Rotameter, 4. Three-way valve Adsorption system, 5. Fixed reactor and water bath, 6. $H_2O_2$ absorption bottle (Detection system), 7. NaOH absorption bottle (Exhaust gas absorption system); (b) schematic diagram of the adsorption column

## RESULTS AND DISCUSSION

### Saturated Sulfur Capacity

The adsorption experiment results of native rice straw, rice straw biochar (RSB), and RSB-MgO adsorbent (ethylenediamine (EDA) as a precipitant) are shown in Fig. 3, and an analysis of the physical properties and elemental compositions of RSB and RSB-MgO are presented in Table 1. The sulfur capacity S.D values of native rice straw, RSB, and RSB-MgO under three parallel experiments were 3.0%, 3.9%, and 4.9% (Fig. 3), all of which are less than 5%, indicating that the data were within experimental errors. Sulfur capacity increased from 5.1 to 11.1 mg/g after the rice straw was carbonized into RSB. After loaded MgO on RSB, the saturated sulfur capacity, BET surface area, and N content of adsorbent increased dramatically from 11.1 to 194.6 mg/g, 10.6 to 138.1 $m^2/g$, and 0.3 to 1.8 %, respectively. This indicated that the RSB-MgO had better desulfurization effect compared with rice straw or rice straw biochar, which was attributed to increase in large specific surface area and N content of adsorbent. The contact time in adsorption process of native rice straw, RSB, and RSB-MgO were 16, 30, and 120 min, respectively, which demonstrated that large specific surface area increased the contact time between $SO_2$ in

adsorbent. In addition, the high saturated sulfur capacity of RSB-MgO was attributed to the basicity and large number of surface active sites (oxygen defects and magnesium defects active) of MgO. The $SO_2$ adsorption performance of MgO depends on these active sites (R. Li *et al*. 2017). The $SO_2$ adsorption on MgO is both physical and chemical adsorption. The physical adsorption of $SO_2$ is dependent on morphology and structure, causing gas molecules to be adsorbed on solid surfaces. In addition, chemical adsorption is related to surface chemical activity, and $SO_2$ may react with MgO to generate $MgSO_3$ at a highly active site. Furthermore, the increased N content in RSB-MgO implied that EDA could have introduced N to RSB-MgO, which promoted $SO_2$ adsorption (Tailor *et al*. 2014b). The results suggested that RSB, MgO, and N content synergistically affect the $SO_2$ adsorption on RSB-MgO. The composite materials of inorganic material and carbon have good desulfurization effect, and the maximum sulfur capacity of $MnO_2$ and $Fe_2O_3$ modified activated carbon were 157.8 and 140.6 mg/g (Fan *et al*. 2013). This proves that MgO enhances $SO_2$ adsorption stronger than $MnO_2$ and $Fe_2O_3$.

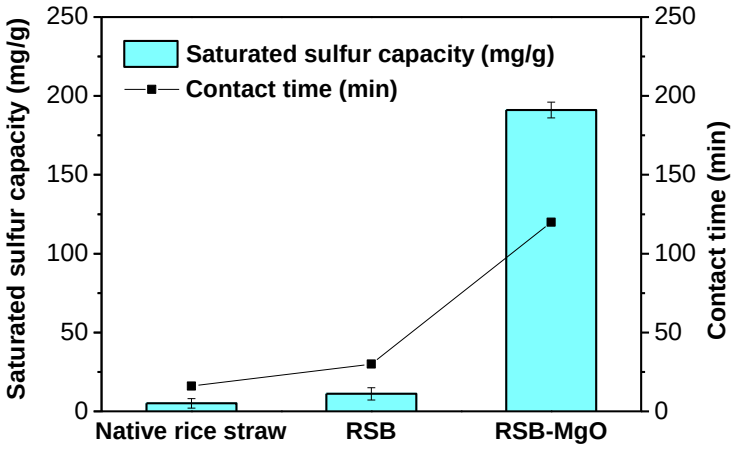


**Fig. 3.** Saturated sulfur capacities of native rice straw, rice straw biochar and RSB-MgO

**Table 1.** Analysis of the Physical Properties and Elemental Composition

| Sample | BET Surface Area ($m^2/g$) | Pore Volume ($cm^3/g$) | Average pore size (nm) | N content (%) | C content (%) | H content (%) |
|---|---|---|---|---|---|---|
| RSB | 10.6 | 0.03 | 12.8 | 0.3 | 48.9 | 2.9 |
| RSB-MgO | 138.1 | 0.4 | 10.3 | 1.8 | 2.0 | 1.6 |

## Effect of Calcination Temperature

Precipitate prepared from rice straw (RS) (2.0 g) and $MgCl_2 \cdot 6H_2O$ (20.33 g, 200 mL) solution was calcined at 300, 400, 500, 600, and 700 °C to obtain RSB-MgO adsorbent. The effect of calcination temperature on the adsorption of $SO_2$ using RSB-MgO was studied using a carrier gas flow rate of 180 mL/min and a heating rate of 15 °C /min. The sulfur adsorption capacities of samples calcined at these five temperatures were 99.0, 194.6, 125.8, 70.6, and 24.2 mg/g, respectively (Fig. 4a), indicating that RSB-MgO adsorbents have good desulfurization performances at various temperatures. The highest sulfur adsorption capacity was observed at 400 °C, and the sulfur capacities were lower on either side of this maximum.

The lower sulfur capacity at 300 °C was due to insufficient carbonization, which

resulted in a large amount of residual lignin and cellulose in the rice straw biochar and a portion of the $Mg(OH)_2$ was not calcined to MgO. When the calcination temperature increased from 400 °C to 700 °C, the ash and carbon loss of rice straw biochar increased, which caused the sulfur capacity to gradually decrease due to excessive carbonization. In addition, increased ash content could have contributed to blocking the pores and active adsorption sites, thus reducing the sulphur capacity. It also increased the crystallite size of MgO due to the sintering of MgO grains.

The XRD patterns of RSB-MgO adsorbents calcined at different temperatures are shown in Fig. 4b. All Bragg diffraction peaks in the XRD patterns were assigned to MgO, which is consistent with bulk MgO crystal (ICSD Patterns-89/59522). Five diffraction peaks corresponding to MgO were identified and indexed to the (111), (200), (220), (311), and (222) crystal planes, corresponding to $2\theta$ values of 36.8°, 42.8°, 62.1°, 74.5°, and 78.4°, respectively. Strong and sharp diffraction peaks indicated highly crystalline MgO particles in the sample. However, the diffraction peaks of $Mg(OH)_2$ were observed in the XRD pattern of RSB-MgO calcined at 300 °C, illustrating that $Mg(OH)_2$ was not completely converted to MgO at 300 °C. The crystallite size ($D$) of the synthesized MgO was calculated from the full width at half maximum (FWHM) of all peaks (111), (200), (220), (311), and (222) using the Debye–Scherrer formula (Makhluf *et al*. 2005),

$$D = \frac{k\lambda}{\beta \cos\theta} \quad (3)$$

where $k$ is the shape factor with a typical value of about 0.9, $\lambda$ is the X-ray wavelength, $\beta$ is the breadth of a diffraction peak at half of its maximum intensity, and $\theta$ is the Bragg angle. The average crystallite sizes of RSB-MgO samples were 16.7, 14.9, 13.8, 14.5, and 16.8 nm (Table 2). The larger crystallite size of MgO calcined at 300 °C was attributed to the coexistence of MgO with incompletely decomposed $Mg(OH)_2$. When the calcination temperature was between 400 °C to 600 °C, MgO crystallites showed a relatively uniform size distribution due to the complete decomposition of $Mg(OH)_2$ into MgO. In contrast, a larger MgO crystallite size at a calcination temperature of 700 °C was caused by the sintering of MgO grains. Therefore, 400 °C was judged to be the most suitable calcination temperature.

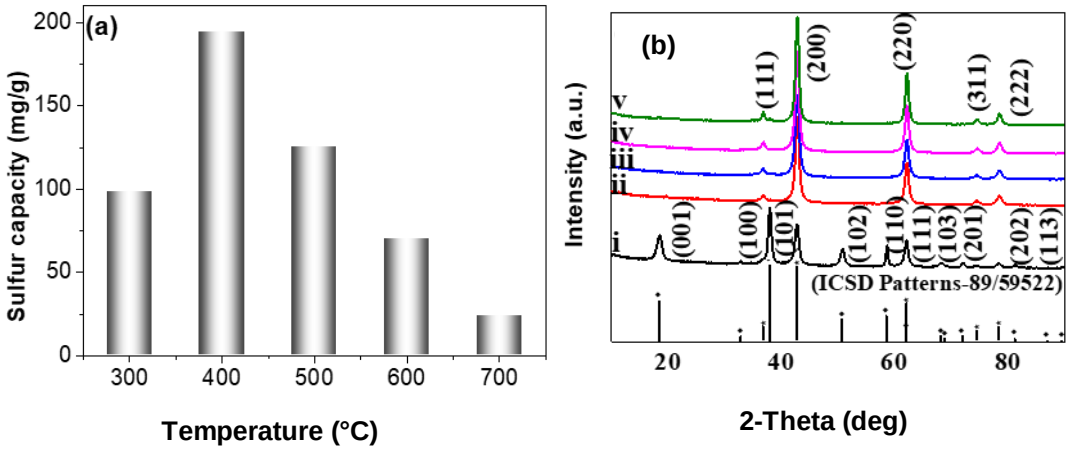


**Fig. 4.** (a) Sulfur adsorption capacity of RSB-MgO at different calcining temperatures, (b) XRD patterns of RSB-MgO adsorbents calcined at different temperatures, (i) 300 °C, (ii) 400 °C, (iii) 500 °C, (iv) 600 °C, (v) 700 °C

**Table 2.** Crystallite Sizes of Different Crystal Planes of RSB-MgO Calcined at Different Temperatures

| Crystal Plane | 2θ (degree) | Crystallite Sizes (nm) | | | | |
|---|---|---|---|---|---|---|
| | | (300 °C) | (400 °C) | (500 °C) | (600 °C) | (700 °C) |
| $d_{average}$ | - | 16.7 | 14.9 | 13.8 | 14.5 | 16.8 |

## Effect of Mg/Rice Straw Weight Ratio

Different masses of rice straw (RS) (2.0 g, 4.0 g, 8.0 g, and 20.0 g) were added to a solution containing $MgCl_2 \cdot 6H_2O$ (20.33 g, 200 mL) to obtain RSB-MgO adsorbent with Mg/RS weight ratios of 1.2, 0.6, 0.3, and 0.1, respectively. The results in Fig. 5 show that increasing the weight ratio of Mg/RS from 0.1 to 1.2 increased the sulfur capacity from 77.9 to 194.6 mg/g. This was attributed to the formation of more vacancies and activation centers on the surface of RSB-MgO due to an increase in the MgO proportion. Therefore, an Mg/RS weight ratio of 1.2 was used in subsequent experiments.

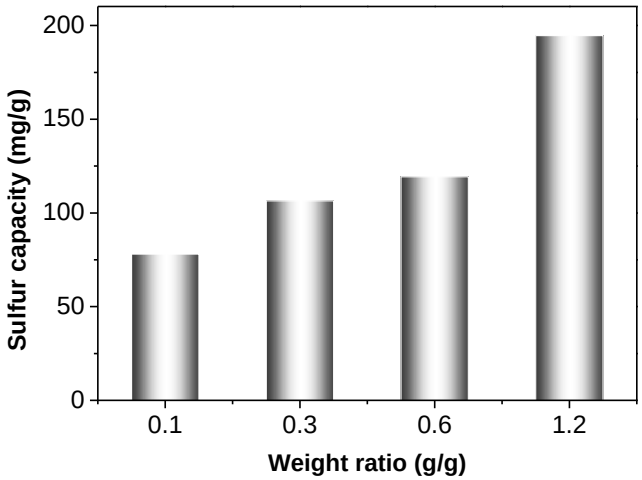


**Fig. 5.** Sulfur capacities of RSB-MgO with Mg/RS weight ratios of 0.1, 0.3, 0.6, and 1.2

## Effect of Magnesium Salts

Chowdhury *et al*. (2016) reported that the anions of different magnesium salts may affect the morphology of MgO crystals. In this work, the effect of different magnesium salts on the $SO_2$ adsorption using RSB-MgO was investigated. Magnesium chloride hexahydrate ($MgCl_2 \cdot 6H_2O$), magnesium nitrate hexahydrate ($Mg(NO_3)_2 \cdot 6H_2O$), and magnesium acetate tetrahydrate ($Mg(CH_3COO)_2 \cdot 4H_2O$) were used as magnesium sources to obtain RSB-MgO. Rice straw (RS) (2.0 g) were added to the solution containing $MgCl_2 \cdot 6H_2O$ (20.33 g, 200 mL), $Mg(NO_3)_2 \cdot 6H_2O$ (25.64 g, 200 mL), and $Mg(CH_3COO)_2 \cdot 4H_2O$ (21.45 g, 200mL), respectively to obtain RSB-MgO adsorbent. The sulfur capacities of the resulting adsorbents are shown in Fig. 6a. RSB-MgO specimens prepared by three different magnesium salts all displayed good desulfurization performances, with respective sulfur capacities of 194.6, 118.0, and 118.4 mg/g. Amongst them, the sulfur capacity of RSB-MgO prepared by $MgCl_2 \cdot 6H_2O$ was much higher than the other two, possibly due to the role of different magnesium salt anions on MgO crystal morphology and crystallinity.

Figure 6b presents the XRD patterns of RSB-MgO samples obtained from different magnesium salts. The same diffraction peaks were observed in all patterns, indicating that

all products were highly pure. The high peak intensity and sharp peak shape of RSB-MgO obtained from $MgCl_2 \cdot 6H_2O$ demonstrates its high crystallinity, which was conducive to $SO_2$ adsorption. The FESEM images of RSB-MgO adsorbents were prepared using $MgCl_2 \cdot 6H_2O$, $Mg(NO_3)_2 \cdot 6H_2O$, and $Mg(CH_3COO)_2 \cdot 4H_2O$ (Figs. 6c, d, e). Clear morphology differences can be observed among samples, and the FESEM images of RSB-MgO formed from $MgCl_2 \cdot 6H_2O$ and $Mg(NO_3)_2 \cdot 6H_2O$ showed circular lamella particles with sizes of 100 nm, while $Mg(CH_3COO)_2 \cdot 4H_2O$ displayed a pleated sheet morphology. The growth of nanocrystals is controlled simultaneously by thermodynamics and kinetics (Hu *et al*. 2010). Different magnesium salt anions could affect the growth rate of crystal and free energy of the crystalline surfaces form different surface morphologies; thus, different surface morphologies of RSB-MgO have different surface properties, which affect the $SO_2$ adsorption on MgO crystalline surfaces. Therefore, $MgCl_2 \cdot 6H_2O$ was the most suitable magnesium source.

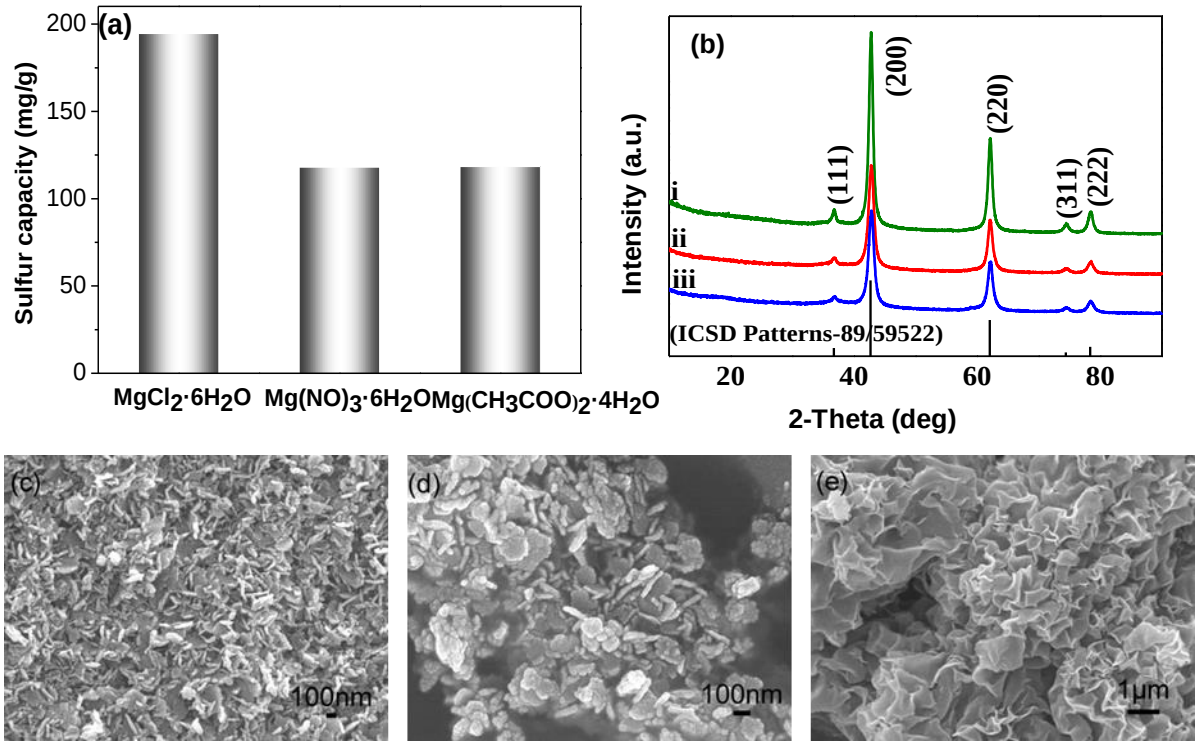


**Fig. 6.** (a) Sulfur capacities of RSB-MgO prepared from different magnesium salts, (b) XRD patterns of RSB-MgO samples prepared from different magnesium salts: (i) $MgCl_2 \cdot 6H_2O$, (ii) $Mg(NO_3)_2 \cdot 6H_2O$, (iii) $Mg(CH_3COO)_2 \cdot 4H_2O$, FESEM images of RSB-MgO prepared from: (c) $MgCl_2 \cdot 6H_2O$, (d) $Mg(NO_3)_2 \cdot 6H_2O$, (e) $Mg(CH_3COO)_2 \cdot 4H_2O$

## Effect of Amine Reagents on Sulfur Capacity

Four amine reagents (ethylenediamine (EDA), tetraethylenepentamine (TEPA), cyclohexylamine (CA), and diethanolamine (DEA)) were used as precipitants and added dropwise respectively to the solution (200 mL) containing rice straw (RS) (2.0 g) and $MgCl_2 \cdot 6H_2O$ (20.33 g) to obtain RSB-MgO-EDA, RSB-MgO-TEPA, RSB-MgO-CA, and RSB-MgO-DEA adsorbents. The resulting sulfur capacities were respectively 194.6 mg/g, 263.6 mg/g, 253.5 mg/g, and 113.5 mg/g (Fig. 7a), showing that all RSB-MgO adsorbents prepared using different amine precipitants have excellent desulfurization effects, but they showed notably different sulfur capacities.

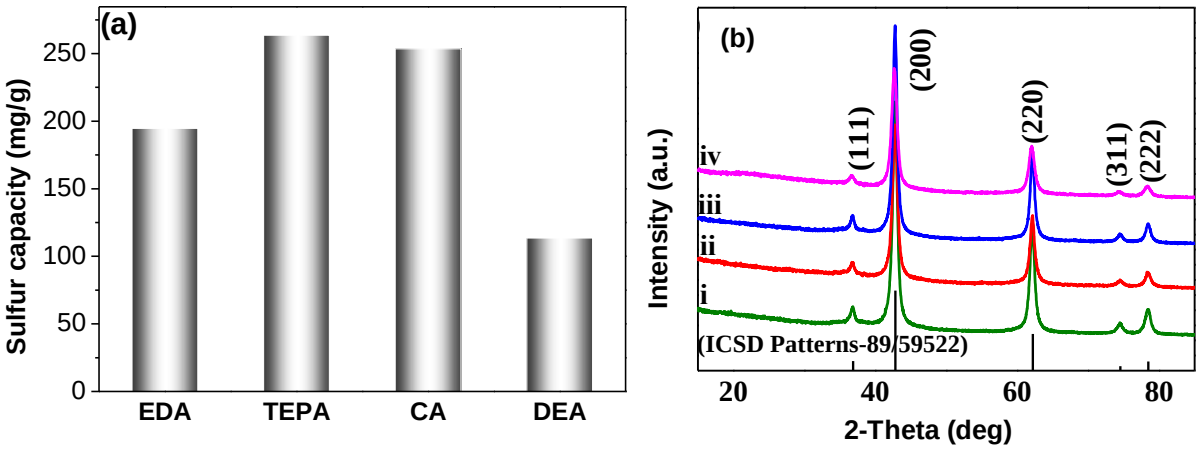


**Fig. 7.** (a) The sulfur capacities of RSB-MgO prepared using different amines, (b) XRD patterns of RSB-MgO prepared using different amine agents, (i) RSB-MgO-EDA, (ii) RSB-MgO-TEPA, (iii) RSB-MgO-CA, and (iv) RSB-MgO-DEA

Table 3 presents the BET parameters (specific surface area, pore volume, and average pore diameter) of RSB-MgO-EDA, RSB-MgO-TEPA, RSB-MgO-CA, and RSB-MgO-DEA. The specific surface areas and pore volumes of these samples considerably increased compared with RSB, which resulted in their higher sulfur capacities. Moreover, the XRD patterns of RSB-MgO-EDA, RSB-MgO-TEPA, RSB-MgO-CA, and RSB-MgO-DEA are presented in Fig. 7 (b). Only diffraction peaks of MgO were detected, indicating that these products were highly pure. The average crystallite sizes were 15.0, 13.8, 14.8, and 12.3 nm, respectively (Table 3). It can be seen that the MgO crystallite size prepared by the amines is DEA (hydroxylamine) <TEPA (long-chain amine) <CA (cyclic amine) <EDA (short-chain amine).

The BET results (Table 3) show that RSB-MgO-TEPA and RSB-MgO-EDA have nearly equal BET surface area values, but RSB-MgO-TEPA exhibited a higher sulfur capacity than RSB-MgO-EDA, which may be related to the smaller crystallite size of RSB-MgO-TEPA. However, the reason why RSB-MgO-CA has a higher sulfur capacity than RSB-MgO-EDA is that RSB-MgO-CA has a smaller crystallite size than RSB-MgO-EDA even though the BET surface area of RSB-MgO-CA was slightly smaller than RSB-MgO-EDA. Therefore, it can be concluded that the smaller crystallite size of adsorbent produced a better desulfurization effect when the BET surface area is not significant difference. It is worth noted that the RSB-MgO-DEA displayed the smaller specific surface area than other three products, which may resulted in a lower number of vacancies and activation sites on its surface, and the main reason why a lower sulfur capacity even though the RSB-MgO-DEA have the smallest crystallite size.

The elemental analysis results in Table 3 show that the nitrogen content of RSB-MgO-EDA, RSB-MgO-TEPA, RSB-MgO-CA, and RSB-MgO-DEA were 1.82%, 1.75%, 1.80%, and 1.85%, respectively, which were all about 6 times higher than that of biochar (0.28%). This indicates that amines were introduced into RSB-MgO, whose alkalinity assisted in the adsorption of acidic $SO_2$. However, the nitrogen content was not significantly different between the samples, indicating that it was not the main influencing factor for the different $SO_2$ adsorptions of RSB-MgO samples prepared using different amines. Moreover, The FT-IR spectra of RSB-MgO-EDA, RSB-MgO-TEPA, RSB-MgO-CA, and RSB-MgO-DEA are presented in Fig 8. The two peaks at 1450 and 1650 $cm^{-1}$ were assigned to N-H deformation and bending vibrations, which demonstrated the

presence of N-H groups in adsorbents. The N-H group may form hydrogen bond with $SO_2$ in the absence of water. It can be concluded that introducing amine groups in RSB-MgO prepared by TEPA long chain amines with multiple amine groups has better $SO_2$ adsorption effect.

**Table 3.** Physical Properties, Elemental Content, Average Crystallite Sizes, and Crystallinity of RSB-MgO Prepared Using Different Amines

| Sample | | RSB | RSB-MgO | | | |
|---|---|---|---|---|---|---|
| | | | EDA | TEPA | CA | DEA |
| Physical properties | BET Surface Area ($m^2/g$) | 10.6 | 138.1 | 139.2 | 120.9 | 69.7 |
| | Pore Volume ($cm^3/g$) | 0.03 | 0.36 | 0.42 | 0.32 | 0.22 |
| | Average pore diameter (nm) | 12.8 | 10.3 | 11.9 | 10.7 | 12.6 |
| | Average crystallite sizes(nm) | - | 15.0 | 13.8 | 14.8 | 12.3 |
| Elemental content | N% | 0.28 | 1.82 | 1.75 | 1.80 | 1.85 |
| | C% | 48.90 | 1.98 | 2.33 | 2.07 | 3.08 |
| | H% | 2.91 | 2.61 | 1.52 | 1.04 | 1.69 |

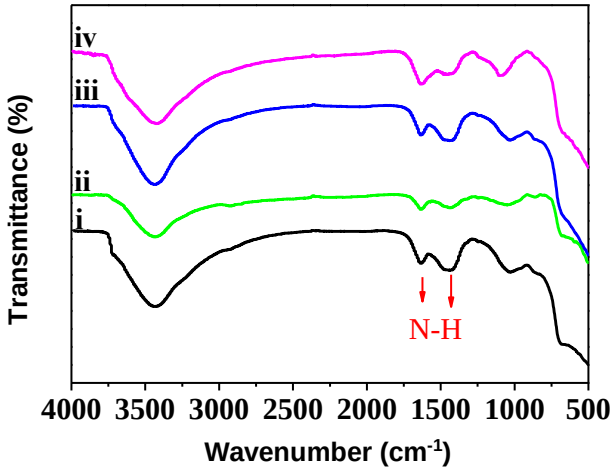


**Fig. 8.** FT-IR spectra of RSB-MgO samples prepared by different amine agents, (i) RSB-MgO-EDA, (ii) RSB-MgO-TEPA, (iii) RSB-MgO-CA, (iv) RSB-MgO-DEA

## Effect of Adsorption Conditions on Sulfur Capacity

*Effect of flow rate of flue gas*

Under the above adsorption experimental conditions (calcination temperature of 400 °C, Mg/rice straw weight ratio of 1.2, $MgCl_2 \cdot 6H_2O$ as magnesium source, tetraethylenepentamine (TEPA) as the precipitant, and adsorption temperatures of 25 °C), the sulfur capacity of the RSB-MgO-TEPA adsorbent was measured with flue gas flow rates of 250, 300, 350, 400, and 450 mL/min (Fig. 9).

Figure 9 shows that RSB-MgO-TEPA had a higher sulfur capacity at a flue gas flow rate of 400 mL/min, while higher or lower flow rates showed similar sulfur capacities. This may be because the lower gas flow rate causes less $SO_2$ molecules to diffuse on the solid adsorbent surface. As the adsorption time increases, the $SO_2$ molecules physically adsorbed on the solid adsorbent surface will desorb, which results the lower sulfur capacity. When increasing the gas flow rate, the gas driving force increased, and the gas driving

force could be assisted in the diffusion and adsorption of $SO_2$ molecules on the solid adsorbent surface. However, when the flue gas velocity was too high, $SO_2$ molecules were ejected without being adsorbed because of short contact time, resulting in a lower desulfurization effect. Therefore, suitable gas flow rate should be selected, 400 mL/min was applied in this experiment.

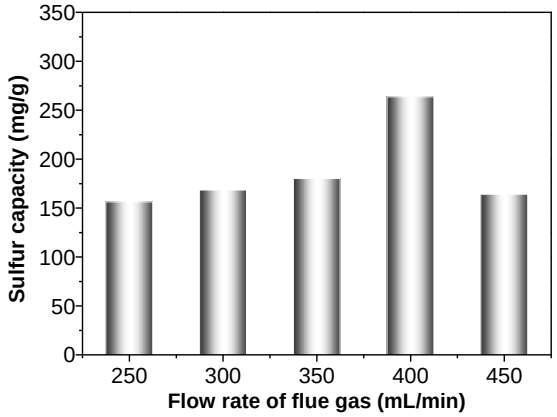


**Fig. 9.** Sulfur capacities of RSB-MgO-TEPA under different flue gas flow rates

*Effect of adsorption temperature*

Under the above adsorption experiment conditions (calcination temperature of 400 °C, Mg/rice straw weight ratio of 1.2, $MgCl_2 \cdot 6H_2O$ as the magnesium source, tetraethylenepentamine (TEPA) as the precipitant, and flue gas flow rates of 400 mL/min), the sulfur capacity of RSB-MgO-TEPA was analyzed at adsorption temperatures of 15, 25, 35, 45, and 55 °C (Fig. 10).

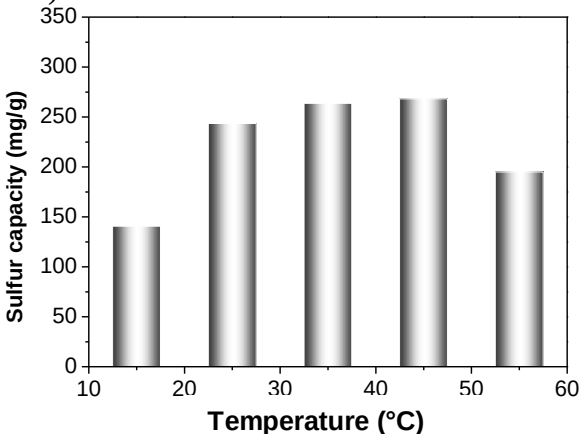


**Fig. 10.** Sulfur capacities of RSB-MgO-TEPA at different adsorption temperatures

Figure 10 shows that when the temperature was raised from 15 °C to 45 °C, the sulfur capacity of RSB-MgO-TEPA gradually increased. When the temperature was further raised to 55 °C, the sulfur capacity decreased, possibly due to the activity of gas molecules. $SO_2$ gas molecules has a low molecular activity at lower temperatures, which caused a high kinetic resistance during diffusion to RSB-MgO-TEPA. As the temperature increased, the activity of $SO_2$ and the amine groups in the adsorbent were enhanced, which was beneficial for the interactions of $SO_2$ with the amine group and diffusion into the adsorbent. However, if the temperature was too high, desorption may occur, resulting in a lower sulfur capacity.

## CONCLUSIONS

1. RSB-MgO adsorbents prepared from the co-precipitation/calcination route displayed excellent desulfurization effects, and sulfur capacities of RSB-MgO adsorbents were much higher than that of native rice straw and rice straw biochar.
2. At a calcination temperature of 400 °C, a Mg/rice straw weight ratio of 1.2, and using $MgCl_2 \cdot 6H_2O$ as the magnesium source and tetraethylenepentamine (TEPA) as the precipitant, the sulfur capacity of the adsorbent reached 260 mg/g at a flue gas flow rate of 400 mL/min and adsorption temperature of 25 °C.
3. The $SO_2$ adsorption was affected by the synergistic action of MgO, rice straw biochar and N-H groups, and MgO played a dominant role in $SO_2$ adsorption.
4. The RSB-MgO-TEPA has a good desulfurization effect because of its circular lamella morphology, large BET surface area, small crystallite size, high crystallinity, and N-H groups introduced.
5. The RSB-MgO adsorbent may be a potential alternative material for $SO_2$ removal in the future, and the use of $MgCl_2 \cdot 6H_2O$ and biomass residues to synthesize $SO_2$ adsorbents provides remarkable economic and environmental advantages.

## ACKNOWLEDGMENTS

The authors gratefully appreciate the use of FESEM, XRD, FT-IR, and EA in the Analytical Testing Center of Sichuan University.

## REFERENCES CITED

Ahmad, M., Rajapaksha, A. U., Lim, J. E., Zhang, M., Bolan, N., Mohan, D., Vithanage, M., Lee, S. S., and Ok, Y. S. (2014). "Biochar as a sorbent for contaminant management in soil and water: A review," *Chemosphere* 99, 19-33. DOI: 10.1016/j.chemosphere.2013.10.071

Al-Harahsheh, M., Shawabkeh, R., Batiha, M., Al-Harahsheh, A., and Al-Zboon, K. (2014). "Sulfur dioxide removal using natural zeolitic tuff," *Fuel Processing Technology* 126, 249-258. DOI: 10.1016/j.fuproc.2014.04.025

Bai, B. C., Lee, C. W., Lee, Y.-S., and Im, J. S. (2016). "Metal impregnate on activated carbon fiber for $SO_2$ gas removal: Assessment of pore structure, Cu supporter, breakthrough, and bed utilization," *Colloids and Surfaces A: Physicochemical and Engineering Aspects* 509, 73-79. DOI: 10.1016/j.colsurfa.2016.08.038

Chowdhury, I. H., Chowdhury, A. H., Bose, P., Mandal, S., and Naskar, M. K. (2016). "Effect of anion type on the synthesis of mesoporous nanostructured MgO, and its excellent adsorption capacity for the removal of toxic heavy metal ions from water," *RSC Advances* 6(8), 6038-6047. DOI: 10.1039/c5ra16837f

Dhal, J., Sethi, M., Mishra, B., and Hota, G. (2015). "MgO nanomaterials with different morphologies and their sorption capacity for removal of toxic dyes," *Materials Letters* 141, 267-271. DOI: 10.1016/j.matlet.2014.10.055

Elder, A. C., Bhattacharyya, S., Nair, S., and Orlando, T. M. (2018). "Reactive adsorption

of humid $SO_2$ on metal–organic framework nanosheets," *The Journal of Physical Chemistry C* 122(19), 10413-10422. DOI: 10.1021/acs.jpcc.8b00999

Fan, L., Chen, J., Guo, J., Jiang, X., and Jiang, W. (2013). "Influence of manganese, iron and pyrolusite blending on the physiochemical properties and desulfurization activities of activated carbons from walnut shell," *Journal of Analytical and Applied Pyrolysis* 104, 353-360. DOI:10.1016/j.jaap.2013.06.014

Guo, J.-x., Liang, J., Chu, Y.-H., Sun, M.-C., Yin, H.-Q., and Li, J.-J. (2012). "Desulfurization activity of nickel supported on acid-treated activated carbons," *Applied Catalysis A: General* 421, 142-147. DOI: 10.1016/j.apcata.2012.02.010

Guo, Y., Li, Y., Zhu, T., Ye, M., and Wang, X. (2013). "Adsorption of $SO_2$ and chlorobenzene on activated carbon," *Adsorption* 19(6), 1109-1116. DOI: 10.1007/s10450-013-9539-y

Huang, Y.-F., Chiueh, P.-T., Shih, C.-H., Lo, S.-L., Sun, L., Zhong, Y., and Qiu, C. S. (2015). "Microwave pyrolysis of rice straw to produce biochar as an adsorbent for $CO_2$ capture," *Energy* 84, 75-82. DOI: 10.1016/j.energy.2015.02.026

Hu, J., Song, Z., Chen, L., Yang, H., Li, J., and Richards, R. (2010). "Adsorption properties of MgO(111) nanoplates for the dye pollutants from wastewater," *Journal of Chemical and Engineering Data* 55, 3742-3748. DOI: 10.1021/je100274e

Jin, Z., Jia, Y., Zhang, K.-S., Kong, L.-T., Sun, B., Shen, W., Meng, F. L., and Liu, J. H. (2016). "Effective removal of fluoride by porous MgO nanoplates and its adsorption mechanism," *Journal of Alloys and Compounds* 675, 292-300. DOI: 10.1016/j.jallcom.2016.03.118

Li, P., Liu, C., Zhang, L., Zheng, S., and Zhang, Y. (2017). "Enhanced boron adsorption onto synthesized MgO nanosheets by ultrasonic method," *Ultrasonics Sonochemistry* 34, 938-946. DOI: 10.1016/j.ultsonch.2016.07.029

Li, R., Wang, J. J., Zhou, B., Zhang, Z., Liu, S., Lei, S., and Xiao, R. (2017). "Simultaneous capture removal of phosphate, ammonium and organic substances by MgO impregnated biochar and its potential use in swine wastewater treatment," *Journal of Cleaner Production* 147, 96-107. DOI: 10.1016/j.jclepro.2017.01.069

Li, Y., Qi, H., and Wang, J. (2012). "$SO_2$ capture and attrition characteristics of a CaO/bio-based sorbent," *Fuel* 93, 258-263. DOI: 10.1016/j.fuel.2011.08.043

Liu, X., Niu, C., Zhen, X., Wang, J., and Su, X. (2015). "Novel approach for the synthesis of Mg (OH) $_2$ nanosheets and lamellar MgO nanostructures and their ultra-high adsorption capacity for Congo red," *Journal of Materials Research* 30(10), 1639-1647. DOI: 10.1557/jmr.2015.113

Makhluf, S., Dror, R., Nitzan, Y., Abramovich, Y., Jelinek, R., and Gedanken, A. (2005). Microwave-assisted synthesis of nanocrystalline MgO and its use as a bacteriocide," *Advanced Functional Materials* 15(10), 1708-1715. DOI: 10.1002/adfm.200500029

Mochida, I., Korai, Y., Shirahama, M., Kawano, S., Hada, T., Seo, Y., and Yoshikawa, M., Yasutake, A. (2000). "Removal of SOx and NOx over activated carbon fibers," *Carbon* 38(2), 227-239. DOI: 10.1016/s0008-6223(99)00179-7

Nassar, M. Y., Mohamed, T. Y., Ahmed, I. S., and Samir, I. (2017). "MgO nanostructure via a sol-gel combustion synthesis method using different fuels: An efficient nano-adsorbent for the removal of some anionic textile dyes," *Journal of Molecular Liquids* 225, 730-740. DOI: 10.1016/j.molliq.2016.10.135

Savage, M., Cheng, Y., Easun, T. L., Eyley, J. E., Argent, S. P., Warren, M. R., Lewis, W., Murray, C., Tang, C. C., Frogley, M. D., *et al*. (2016). "Selective adsorption of sulfur dioxide in a robust metal–organic framework material," *Advanced Materials* 28(39),

8705-8711. DOI: 10.1002/adma.201602338

Sun, L., and Zhu, X. (2018). "Practical and theoretical study of the adsorption performances of straw-based tertiary amine-supported material toward sulfur dioxide in flue gas," *BioResources* 13(1), 1132-1142.

Tailor, R., Abboud, M., and Sayari, A. (2014a). "Supported polytertiary amines: highly efficient and selective $SO_2$ adsorbents," *Environmental science & technology 48*(3), 2025-2034. DOI: 10.1021/es404135j

Tailor, R., Ahmadalinezhad, A., and Sayari, A. (2014b). "Selective removal of $SO_2$ over tertiary amine-containing materials," *Chemical Engineering Journal* 240, 462-468. DOI: 10.1016/j.cej.2013.11.002

Tan, K., Zuluaga, S., Wang, H., Canepa, P., Soliman, K., Cure, J., Li, J., Thonhauser, T., and Chabal, Y. J. (2017). "Interaction of acid gases $SO_2$ and $NO_2$ with coordinatively unsaturated metal organic frameworks: M-MOF-74 (M= Zn, Mg, Ni, Co)," *Chemistry of Materials* 29(10), 4227-4235. DOI: 10.1021/acs.chemmater.7b00005

Vellingiri, K., Kim, K.-H., Kwon, E. E., Deep, A., Jo, S.-H., and Szulejko, J. E. (2016). "Insights into the adsorption capacity and breakthrough properties of a synthetic zeolite against a mixture of various sulfur species at low ppb levels," *Journal of Environmental Management* 166, 484-492. DOI: 10.1016/j.jenvman.2015.10.053

Vu, A.-T., Ho, K., Jin, S., and Lee, C.-H. (2016). "Double sodium salt-promoted mesoporous MgO sorbent with high $CO_2$ sorption capacity at intermediate temperatures under dry and wet conditions," *Chemical Engineering Journal* 291, 161-173. DOI: 10.1016/j.cej.2016.01.080

Wang, A., Fan, R., Pi, X., Zhou, Y., Chen, G., Chen, W., and Yang, Y. L. (2018). "Nitrogen-doped microporous carbons derived from pyridine ligand-based metal-organic complexes as high-performance $SO_2$ adsorption sorbents," *ACS Applied Materials & Interfaces* 10(43), 37407-37416. DOI: 10.1021/acsami.8b12739

Wang, X., Ma, X., Zhao, S., Wang, B., and Song, C. (2009). "Nanoporous molecular basket sorbent for $NO_2$ and $SO_2$ capture based on a polyethylene glycol-loaded mesoporous molecular sieve," *Energy and Environmental Science* 2(8), 878-882. DOI: 10.1039/b906476a

Wu, W., Yang, M., Feng, Q., McGrouther, K., Wang, H., Lu, H., *et al*. (2012). "Chemical characterization of rice straw-derived biochar for soil amendment," *Biomass and Bioenergy* 47, 268-276. DOI: 10.1016/j.biombioe.2012.09.034

Xu, X., Huang, D., Zhao, L., Kan, Y., and Cao, X. (2016). "Role of inherent inorganic constituents in $SO_2$ sorption ability of biochars derived from three biomass wastes," *Environ. Sci. Technol.* 50(23), 12957-12965. DOI: 10.1021/acs.est.6b03077

Yan, Z., Liu, L. L., Zhang, Y. L., Liang, J. P., Wang, J. P., Zhang, Z. T., and Wang, X. (2013). "Activated semi-coke in $SO_2$ removal from flue gas: Selection of activation methodology and desulfurization mechanism study," *Energy and Fuels* 27(6), 3080-3089. DOI: 10.1021/ef400351a

Yan, Z., Wang, J., Zou, R., Liu, L., Zhang, Z., and Wang, X. (2012). "Hydrothermal synthesis of $CeO_2$ nanoparticles on activated carbon with enhanced desulfurization activity," *Energy and Fuels* 26(9), 5879-5886. DOI: 10.1021/ef301085w

Yang, C., Tan, T., and Zhu, X. (2012). "Adsorptive capacity of ethylenediamine treated oxidised rice straw for sulfur dioxide," *Carbohydrate Polymers* 87(2). DOI: 10.1016/j.carbpol.2011.10.013

Yi, H., Wang, Z., Liu, H., Tang, X., Ma, D., Zhao, S., Zhang, B., Gao, F., and Zuo, Y. (2014). "Adsorption of $SO_2$, NO, and $CO_2$ on activated carbons: Equilibrium and

thermodynamics," *Journal of Chemical and Engineering Data* 59(5), 1556-1563. DOI: 10.1021/je4011135

Zhou, J., Yang, S., and Yu, J. (2011). "Facile fabrication of mesoporous MgO microspheres and their enhanced adsorption performance for phosphate from aqueous solutions," *Colloids and Surfaces A: Physicochemical and Engineering Aspects* 379(1-3), 102-108. DOI: 10.1016/j.colsurfa.2010.11.050

Zhou, X., Yi, H., Tang, X., Deng, H., and Liu, H. (2012). "Thermodynamics for the adsorption of $SO_2$, NO and $CO_2$ from flue gas on activated carbon fiber," *Chemical Engineering Journal* 200, 399-404. DOI: 10.1016/j.cej.2012.06.013

Article submitted: January 8, 2020; Peer review completed: April 3, 2020; Revised version received and accepted: April 19, 2020; Published: May 5, 2020.
DOI: 10.15376/biores.15.2.4738-4752